A numerical model for predicting powder characteristics in LMD considering particle interaction

GUNER, Ahmet, BIDARE, Prveen <http://orcid.org/0000-0003-2852-3498>, JIMÉNEZ, Amaia, SHU, Chang, KOVACEV, Nikolina and ESSA, Khamis

Published version

GUNER, Ahmet, BIDARE, Prveen, JIMÉNEZ, Amaia, SHU, Chang, KOVACEV, Nikolina and ESSA, Khamis (2024). A numerical model for predicting powder characteristics in LMD considering particle interaction. Advanced Powder Technology, 35 (3): 104348.

Advanced Powder Technology 35 (2024) 104348

Contents lists available at ScienceDirect

Advanced Powder Technology

journal homepage: www.elsevier.com/locate/apt

A numerical model for predicting powder characteristics in LMD considering particle interaction

Ahmet Guner [a], Prveen Bidare [b], Amaia Jiménez [c,*], Chang Shu [a], Nikolina Kovacev [a], Khamis Essa [a,*]

[a] School of Mechanical Engineering, University of Birmingham, Birmingham, UK
[b] Department of Engineering and Mathematics, College of Business, Technology and Engineering, Sheffield Hallam University, Sheffield S1 1WB, UK
[c] Universidad de Navarra, TECNUN Escuela de Ingeniería, Manuel de Lardizábal 15, 20018, San Sebastián, Spain

ARTICLE INFO

Article history:
Received 20 October 2023
Received in revised form 11 January 2024
Accepted 29 January 2024

Keywords:
Additive manufacturing
Coaxial nozzle
Directed energy deposition
Agglomeration
Particle adhesion

ABSTRACT

In this work, a numerical model is proposed to analyze the influence of particle–particle interaction in laser directed energy deposition or LMD (laser metal deposition) of CM247 Ni-based superalloy. The model is based on the analysis of contact between particles and the potential agglomeration of powder to predict powder conditions at the nozzle exit. Simulation results were experimentally validated and a good agreement was observed. At the nozzle exit mainly large particles (>100 μm) are found and small ones (<10 μm) tend to flow away from this region. This was also observed in the experimental PSD. Additionally, based on the relative velocity of particles, simulations are able to predict the formation of dents. In comparing virgin powder PSD and the one at the nozzle exit, it was observed that largest particles are collected at the exit. In order to explain this phenomena, particle agglomeration was analysed numerically. It was seen that small particles tend to adhere to the big ones due to their higher adhesive forces, which would explain the change in PSD.

1. Introduction

Laser metal deposition (LMD) technology is one of the most employed and studied Metal Additive Manufacturing (MAM) processes [1]. It is mainly employed for the generation of near-net-shape components, but it can also be applied for material coating and for the repair of damaged or worn components. LMD consists on the deposition of melted powders layer-by-layer for the manufacturing of components [2,3]. Fig. 1 shows a schematic diagram of this AM technology. As it is seen, in LMD a laser is employed as heat source to melt the powders. As shown in Fig. 1, powder and gas are delivered through a deposition nozzle that can have several configurations and shapes [4]. Among the different nozzle designs, the continuous coaxial nozzle design is the most common industrial solution. This nozzle configuration has shown the best performance for the deposition of narrow tracks and also regarding the powder catchment efficiency. During the process, carrier gas and shielding gas are used to deliver powder and avoid metal oxidation, respectively. Powders along with carrier gas and shielding gas are delivered through different external channels in the nozzle while the laser and inner shieling gas are located in an inner channel. This inner shielding gas has the main aim of protecting the optical system from bounced powders and metal vapours [5].

Although the use of MAM technologies has increased dramatically during the last few years, there is still much work to accomplish in order to fully understand the influence of each parameter involved and to control and optimize the process. Considering this, numerical modelling of the process can provide an insight to the different phenomena that occur during LMD. In AM processes, lots of different thermo-mechanical and physical phenomena occur simultaneously and researchers have made efforts to model them in order to better understand and control the process performance.

The first models found in the literature are analytical models that focused on different phenomena occurring in the process. Lin [6] predicted powder concentration based on a mathematical model that included the diffusion and convection models of powder in a gaseous medium. However, this model does not consider the influence of nozzle geometry and of shielding and carrier gas flows. This same author also studied the attenuation of laser powder as consequence of the shadowing effect of the powders based on the Bouguer-Beer law for two different coaxial nozzle arrangements; i.e., inward and outward configurations [7]. He observed that catchment efficiency is not significantly improved by a

* Corresponding authors.
E-mail addresses: ajzabaleta@tecnun.es (A. Jiménez), k.e.a.essa@bham.ac.uk (K. Essa).

https://doi.org/10.1016/j.apt.2024.104348

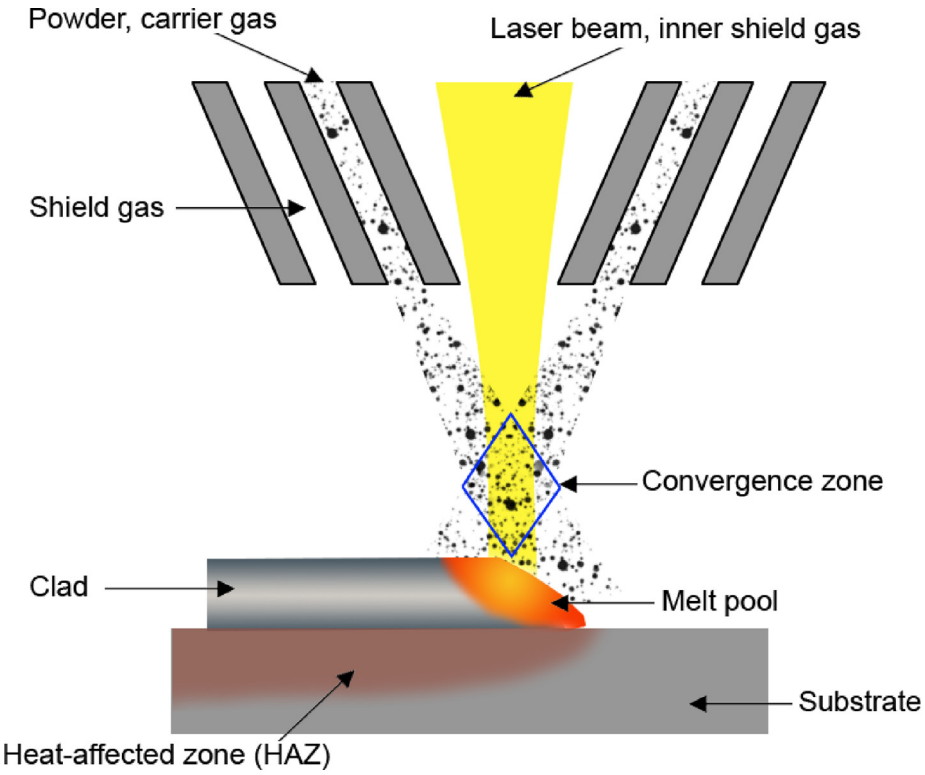

Fig. 1. Schematic diagram of LMD process.

focused stream due to the high laser energy consumption that occurs in this case.

In the last decade, numerical models have been employed to analyze the process as they enable the integration of different physical phenomena much more efficiently. Some works in the literature analyze the influence of nozzle geometry on the resulting powder stream and on the location of the focus point [8]. Lin himself developed a numerical model to analyze focused powder streams generated in LMD process with coaxial nozzle [9]. In 2005, Pan et al. [10] considered the influence of powder morphology on the obtained powder stream characteristics at the exit of a coaxial nozzle. However, they did not consider the effect of the carrier gas flow. Authors also employed their model to analyze the influence of nozzle geometry on the powder stream and concluded that the width and the outer diameter of the powder outlet passage have the greatest effect on the powder stream. Later these authors published another study [11] in which the effects of inner and outer shielding gasses and nozzle geometrical parameters on powder stream were simulated numerically. In the last work, the nozzle angle was included as variable in the model and they observed that smaller angles lead to a more focused powder stream. As one relevant conclusion authors pointed out that powder passage configuration and outer shielding gas must be optimized to ensure best laser energy utilization. Li et al. [12] simulated numerically LMD process in coaxial nozzles and studied the influence of nozzle geometry and configuration and powder feeding parameters on the characteristics of the converging region. They concluded that an increase in powder passage length improves the convergence. They also observed that uniformly sized powders lead to smaller convergence zones. Regarding the nozzle configuration, continuous coaxial nozzles achieve better convergence when compared to discrete coaxial nozzles. More recently, Xia et al. [13] a analyzed the feasibility of a new type of annular coaxial nozzle that transforms a 4-channel powder flow into a more uniform annular powder distribution. Based on a two-way turbulence coupling method, authors simulated the powder transport, convergence and concentration distribution and deposition performance of the nozzle. Zkovis et al. [14] developed a 3D model of the powder-gas flow in a radially symmetrical nozzle considering turbulent flow. Additionally, they employed a different modelling approach to simulate the flow in the region near to the nozzle wall, where the viscosity affects the characteristics of the flow. Wen et al. [15] also considered a turbulent model for simulating the powder and gas flows inside and out of the nozzle. Additionally, these authors also predicted the powder temperature evolution by considering the interaction between powders and laser beam. As in other research works presented above, they included the influence of powder morphology and size distribution in the process modelling. Zhang et al. [16] employed the gas–solid two-phase theory to simulate the flow field inside and out of the nozzle. They observed that for a given cone angle, if the cone ring gap decreases, the focusability of the stream is improved. On the other hand, given an invariable cone ring, if the cone angle acquires either too big or small values, the focusability of the powder is decreased. Finally, they also analyzed the influence of shielding gas velocity and observed that extreme values of this parameter also deteriorate the powder focusabilty. Morville et al. [17] developed a numerical model that considered dynamic and thermal behavior of LMD process with coaxial nozzle. This model considered collisions of powder with the nozzle wall and gas drag to predict the position of the powder stream focal point. The model was employed considering two different powders with different powder weights and authors noted that heavier powders reach the focus point closer to the nozzle exit. Another important conclusion of this work is that collision of the powders changes the structure of the powder size distribution and shape. It is also known that the density of the powders is changing the focal point distances. More recently, Takemura et al. [18] employed a CFD model to analyze the influence of gas-flow and nozzle geometry on the convergence of powder. They observed that convergence improves with higher carrier gas flow rates and convergence

distance must be increased when high carrier flow rates are employed to maintain good powder convergence levels. Additionally, the suggested that sputter of powders and powder-flow convergence must be considered simultaneously when studying powder convergence.

Modelling of LMD has also been conducted with the aim of understanding and controlling the resulting component microstructure. As an example of this, Nie et al. [19] integrated CFD modelling of the powder trajectories, physical energy function to predict laser energy absorbed by the powder and FEM modelling of LMD process. In 2019, Khamidullin et al. [20] analyzed the influence of powder size distribution on the shape and dimensions of the deposition, the heat affected zone and the non-melted powders. Along with other phenomena, their model included the prediction of metal crystal micro-structure during the solidification of the deposition.

With regard to the powder employed in these technologies, argon atomization and the plasma rotating electrode process are the two main technologies used to produce powders. Due to its ability to balance price and powder properties, the argon atomization technology has significant industrial applications in the field of advanced material processing and manufacturing. However, the uniformity and stability of the powder spreading during the additive manufacturing are likely to be significantly affected by satellites on powders which will affect particle non-sphericity [21]. Works in the literature try to model powder behavior considering different interactions. Sinclair at al. [22] used 150 μm powders and found that inelastic interactions between powders are capable of producing segregation. Xiao-Yang Sun et al. [23] studied the performance of Al_2O_3 particles and showed that at 27 m/s speed powder particles of 150 μm size could erode surface in pipe erosion. They also noted that powder flowing at 5 m/s and considering 90° collisions can suffer fragmentation and with velocities higher than 25 m/s, breakage of all particles occur [24]. Rozenblat et al. [25] studied particle breakage under impact load conditions and define the specific impact velocity from which powder breaking takes place.

From the literature review presented above, it is clear that many attempts using numerical simulations of LMD process have been made to understand the influence of process variables on the powder flow behavior. However, the analysis of powder interaction with the nozzle and between particles, powder characteristics at the nozzle exit and powder agglomeration that may influence process performance and obtained component properties and quality is still missing in the literature. The present paper is aimed at analyzing the powder stream flow inside the nozzle taking into account (1) the inner and outer shielding gas and carrier gas flows, (2) the collisions between powders and with the nozzle walls, and (3) dent formation and agglomeration of the powder particles as consequence of the collisions. Concretely, the model focuses on the powder delivery system inside the nozzle and how this affects the powder flow at the exit and powder flows in LMD chamber. The main objective of the model is to predict possible powder agglomeration and dent formation that may alter powder morphology, modify powder PSD at the nozzle exit and, in turn, influence the process performance. It is worth noting that powder deposition and melt pool characteristics, the effect of particle non-sphericity, turbulent wakes behind powders and the effect of dispersed phase packing are beyond the scope of this study and are not analyzed here.

2. Materials and methods

As mentioned, in this work numerical simulations of powder flow during LMD process were conducted taking into account selected process parameters, powder morphology, size, material properties and interaction between particles. The performance predicted by the simulations has been experimentally validated. In this section, details about the numerical models employed and the experimental tests conducted are given.

2.1. Numerical simulation

To simplify the calculation, in this study, one-way coupling is used to simulate the gas and gas–solid flow. The powder stream was coupled as a discrete phase in the Euler-Lagrange model, which has already been proven to be an effective method in earlier similar research. The gas phase was calculated using the widely accepted standard k-ε turbulent flow model. Additionally, the following assumptions and simplifications were considered for the CFD simulations in the proposed model:

- Continuous phase consists of the inner shield, carrier and shield gas while the powders operate as a discrete phase into the continuous phase.
- CFD-DEM coupling is done in one-way. The fluid field influences the flow of the powders. Due to the low mass and concentration of the powders, the discrete flow of powder does not affect the continuous phase.
- The model takes into account the forces of drag, inertia, and gravity while ignoring other factors like acceleration of the surrounding flow.
- Substrate and powder materials are assumed as solid and homogeneous.
- All powders are considered perfectly spherical and powder sizes are defined considering the PSD of the virgin powder that was measured experimentally. For the simulations, a PSD distribution of 1–130 μm was considered. Further details about powder size are given in the following section.
- The dimensions of the nozzle were defined based on those of a real coaxial nozzle fitted into Mazak i-400AM machine (see Fig. 2).
- The gas flow and powder velocity are assumed to be constant and perpendicular to the nozzle's inlet surface at the gas and gas-powder inlets.
- Laser melting or deposition simulation is not considered in this system since it does not influence powder flow from the nozzle. Thus, the heat transfer is not included in the model but because of power-powder interaction occur in powder flow, thermal softening and inelastic collision is applied to powders while calculating dent formation.
- The collision among powders in the passage of the nozzle is included.
- The gravitational effect on the powder is included.
- As for the gas sources, default properties of argon gas are employed.

The particle's absolute velocities can be 0 in a fluid by setting the X, Y, and Z components of velocities to zero. Particles are then accelerated in accordance with their force balance. So the inlet velocity of the particles is taken as relatively zero, and the flow rate is set as 8 g/min. To analyze the influence of argon gas flow and the powder size a gas–solid multiphase flow simulation model is conducted by using Ansys Fluent. The trajectory of each powder particle is described in a Lagrangian reference frame based on a force balance. The momentum loss when particles collide with internal walls of the nozzle is evaluated by a restitution coefficient, which is defined as the ratio of velocities before and after collision [26]:

$$e_n = \frac{u_1}{u_0} \tag{1}$$

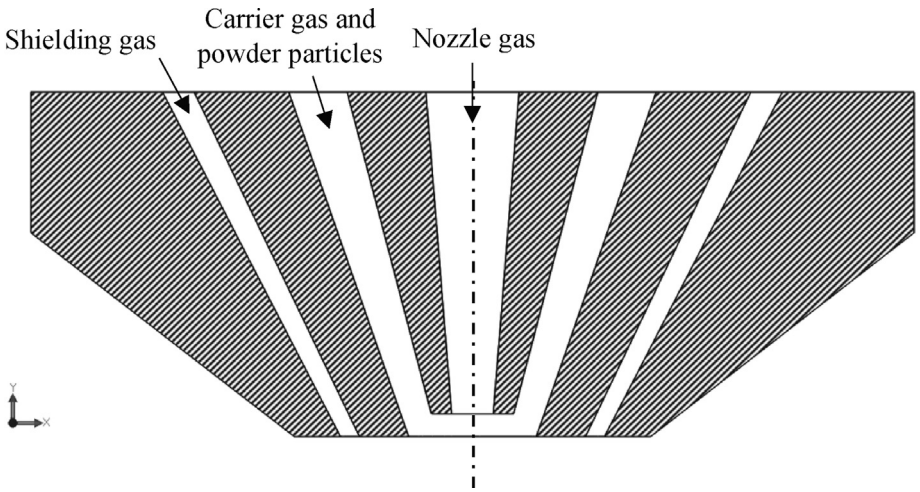

Fig. 2. Schematic diagram of the LMD nozzle geometry considered in this work.

where u_0 and u_1 refer to velocities before and after a collision, respectively. The momentum is lost in an inelastic collision when $e_n < 1$. Restitution coefficient, in general, depends on the material of the powder and nozzle, the impact velocity, the hardness ratio, and the roughness of the nozzle wall [27,28]. In this study, a restitution coefficient of 0.3 was assumed at the beginning of the simulation for all powder particles.

Fig. 3 shows a flow diagram of the steps followed in the proposed approach. As mentioned above, particle–particle interaction is analyzed in this study as it can change powder morphology and, in turn, process performance. As shown in the figure, the results from the simulations are the prediction of dent formation (particle deformation) and particle agglomeration in LMD process based on the resulting stress fields.

As initial input, process parameters such as powder material, its properties and PSD and powder flow characteristics (powder feed rate, carrier gas flow, etc.) are needed. Table 1 and Table 2 show the process parameters considered and powder characteristics. With these parameter values, powder particle velocities are calculated first through Ansys Fluent software. Parameter values employed for the simulations were also employed in the experimental tests for validation.

Table 1
Process parameter values employed for particle velocity calculation.

Nozzle Gas Flow	Carrier Gas Flow	Shield Gas Flow	Powder Flow
Ar (5 L/min)	Ar (6 L/min)	Ar (7 L/min)	CM247LC (8 g/min)

Then, powder particles are forced to collide and considering the relative velocity between particles, stress field for a certain particle is calculated based on the Johnson - Cook plasticity model [26]. Dent formation is predicted next taking into account the powder material mechanical properties through the calculation of plastic deformation that are consequence of those stresses. Johnson Cook model was integrated in the simulations conducted in Ansys software for the calculation of plastic deformations. This model defines the yield stress Y as follows:

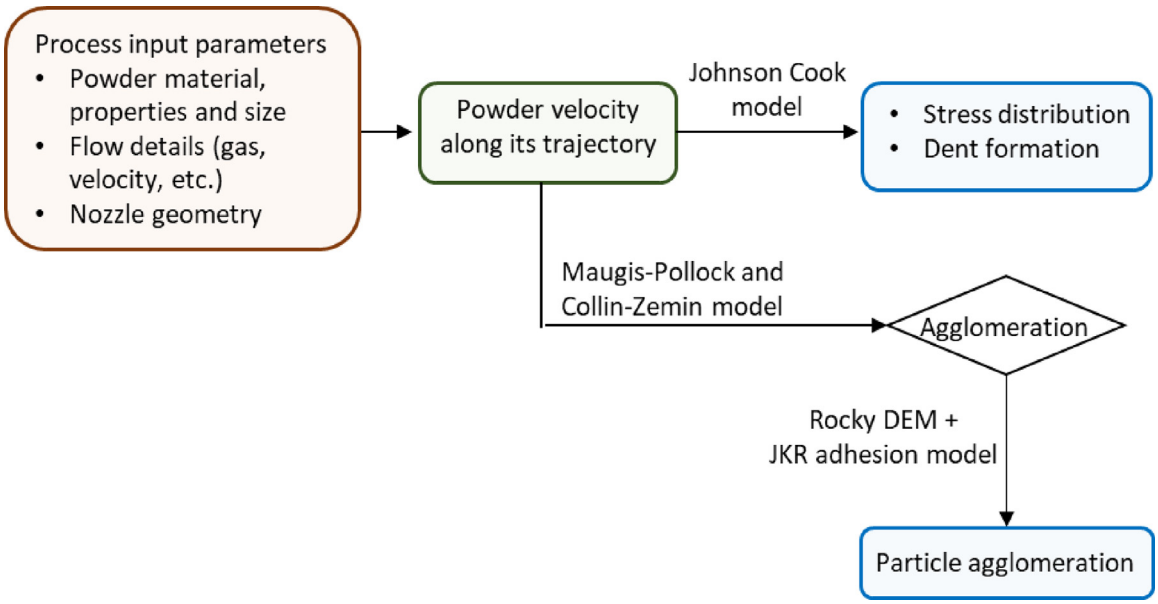

Fig. 3. Flow diagram of the approach proposed in this work.

Table 2
Composition (wt, %) of the CM247LC powder used in this research.

C	Al	Ti	Cr	Mo	Hf	Ta	Co	W	B	N	O	O(supplier)	Ni
0.09	5.57	0.80	8.29	0.67	1.31	3.10	9.59	9.57	140 ppm	<20 ppm	<100 ppm	75 ppm	Bal.

$$Y = \left[A + B\varepsilon_p^n\right]\left[1 + C\ln\varepsilon_p^*\right]\left[1 - T_H^m\right] \quad (2)$$

where ε_p is the effective plastic strain, ε_p^* is the normalized effective plastic strain rate and T_H refers to the homologous temperature: $(T - T_{Room})/(T_{Melt} - T_{Room})$

A, B, C, n and m are parameters that depend on the material. In this work CM247 nickel-based alloy was employed for the experiments. Johnson Cook model parameters corresponding to this alloys group are summarized in Table 3 [29].

In parallel, potential adhesion between particles is studied. Based on Maugis-Pollock and Collin-Zemin model [30-33] the possible agglomeration of powder particles is evaluated. If this last study concludes that powder particles may agglomerate under the given velocity conditions, by employing Rocky DEM simulation and Johnson-Kendall-Roberts (JKR) model [34] for adhesion force calculation, agglomeration of particles is predicted and simulated. In order to calculate the normal and tangential forces arising, the Hertzian Spring Dashboard model and Linear Spring Coulomb models were considered in Rocky DEM. Adhesive forces were calculated based on JKR model and an adhesive particle – particle interaction parameter of 1 J/m^2 was set for the simulation. The rest of parameters were set as default.

It is worth noting here that, unlike what is done in other studies, in this study powder motions are not stopped after colliding to the tube walls and small powders keep flowing even inside the tube. An imaginary chamber that covers the nozzle and the tube is added to the simulation in order to stop powder motion and remove them from calculation.

2.2. EXPERIMENTAL TESTS

To validate the results obtained in the model, powder flow was performed through the LMD nozzle over with a 5.76 mm inner hole diameter (see Fig. 4). Distance between nozzle outlet and powder stream focus plane was set to 10 mm as recommended by machine manufacturers. The aim of this tests is to collect the powder spread along the radial direction and analyze the variation of PSD from the center to the outers of the powder.

According to the powder employed in the experiments, Fig. 5 (a) shows a SEM image of the virgin CM247 powder that will be later compared to the powder collected on the tubes during the experimental tests to analyze the formation of dents and agglomeration of particles. It is observed that virgin powders have a spherical shape with size variety. PSD of the virgin powder is shown in Fig. 5 (b). As it is seen, a bimodal powder was employed for the experiments, where most of the powder particles have 30 μm (small size particles) or 110 μm (large size particles) diameters.

In order to validate the flow calculated by the simulation, Schlieren imaging of the shielding gas was also conducted. Fig. 6 shows a scheme of the setup employed for the Z-Type Schlieren imaging [35]. Those images were focused on the deposition area in order to capture the shape and dimensions of the convergence zone to compare it with the simulated CFD results. The setup

Table 3
Johnson-Cook model parameter values for nickel-based alloys.

A (MPa)	B (Mpa)	C	n	m
1108	699	0.015	0.5189	1.2861

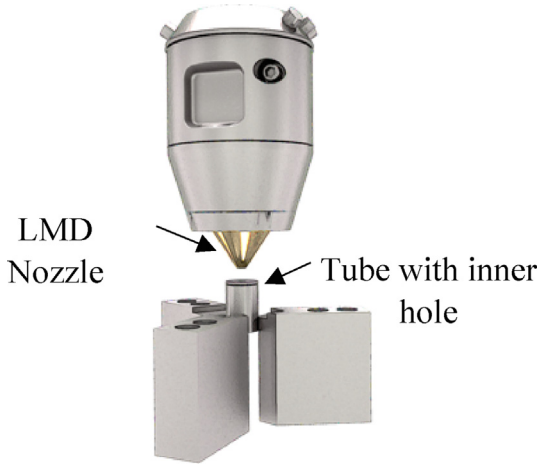

Fig. 4. Schematic diagram of the experimental setup.

was made up of a LED light bulb with a pin hole, two concave mirrors (100 mm in diameter with 75 mm focal length), a knife edge and a FLIR DSLR type digital camera with a telephoto lens (focal length of 55–200 mm). Yellow arrows indicate the light source which goes to first concave mirror to obtain the parallel light area between two mirrors (blue arrows). This area is used to visualize the density difference in flow media. Second concave mirror reflects the light and send them to its focal point (red arrows). Finally, the knife edge is positioned at the focal point of the light and Schlieren images are recorded with FLIR camera.

3. Results and discussion

In this section, results obtained from the experimental tests and those form the numerical simulations are presented.

3.1. CFD SIMULATION OF POWDER FLOW

Fig. 7 shows a comparison of the shielding gas flow predicted by the model (a) and the one experimentally captured through Schlieren imaging (b). Dotted lines in both figures represent the boundaries of the gas flow. It can be observed that the shape of these boundaries match in both cases.

Regarding the sizes of particles collected in the tubes on the experimental tests, Fig. 8 shows a comparison of PSDs from the virgin powder (blue), the simulated powder (yellow) and the experimentally collected powder (grey).

It is seen that the PSD simulated fits almost perfectly with the one from the virgin powder. However, the powder collected during the experimental tests differs slightly from them. PSD of particles collected in the tube show that a higher number of big particles with a 130 μm approximate size reach the tubes. In the following section, numerical simulations conducted in this study will be presented. These simulations are aimed to explain, among other issues, the lack of small size particles at the nozzle exit noticed in the experimental analysis and the difference on PSD between the virgin powder and the one collected from the tube tests.

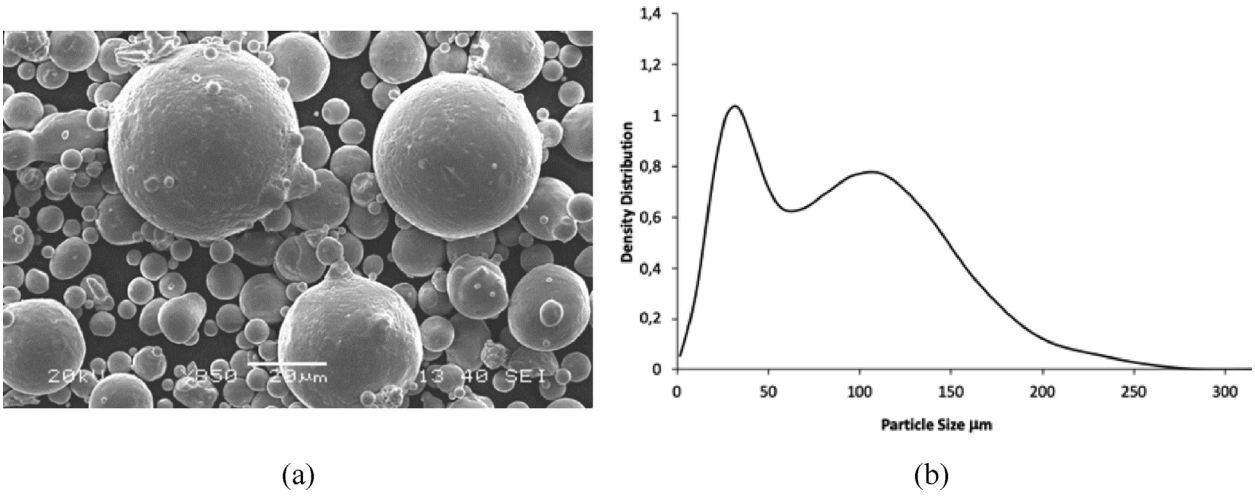

Fig. 5. Virgin powder: (a) morphology and (b) PSD.

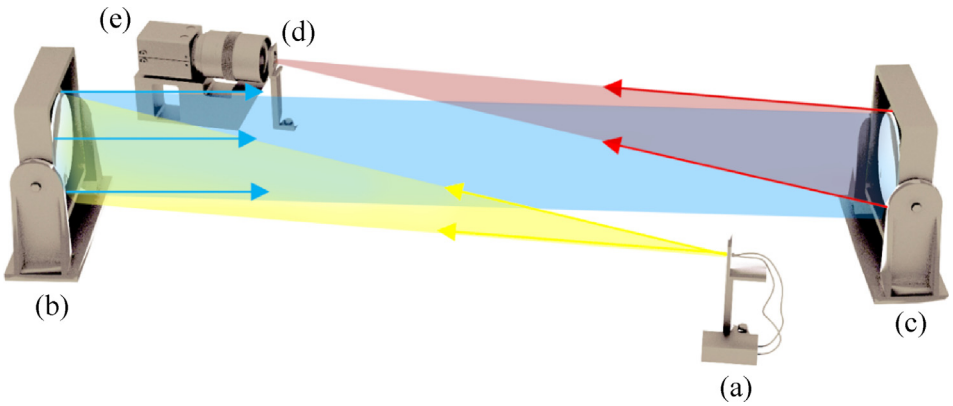

Fig. 6. Setup employed for the Z-Type Schlieren imaging: (a) light source, (b) concave mirror 1, (c) concave mirror 2, (d) knife edge and (e) FLIP camera.

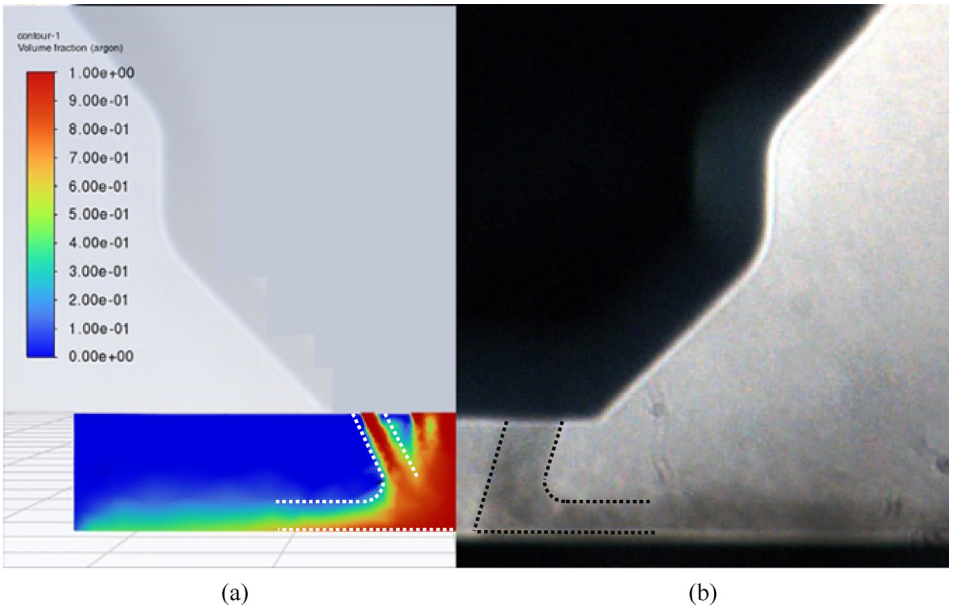

Fig. 7. Schlieren image of the Argon gas flow (shielding gas): (a) numerical simulation and (b) experimentally captured.

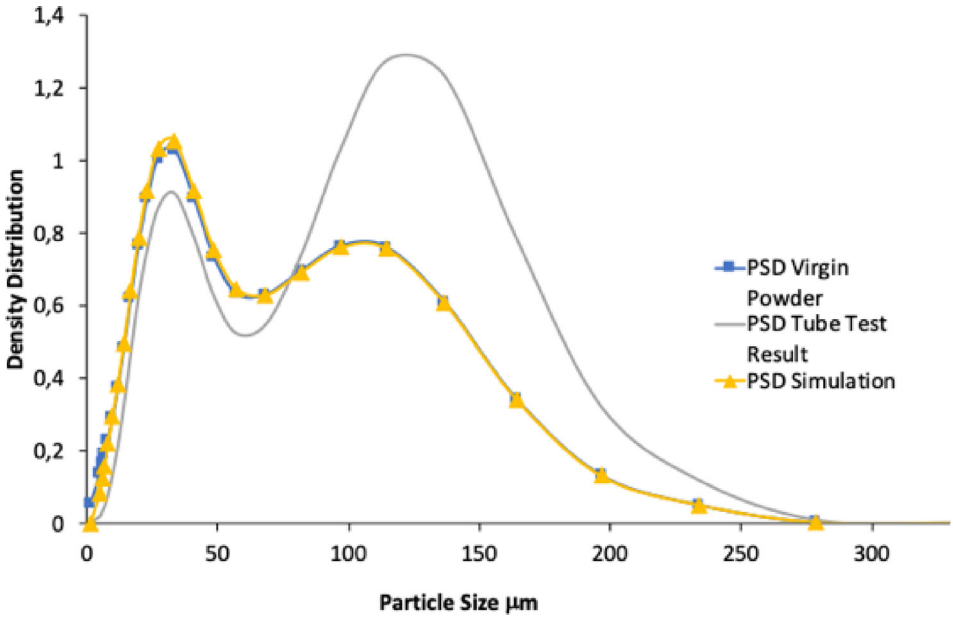

Fig. 8. PSD of the virgin (blue), simulated (yellow) and experimentally collected (grey) powder. (For interpretation of the references to color in this figure legend, the reader is referred to the web version of this article.)

Fig. 9 shows the predicted path of 1 µm (blue) and 130 µm (red) powder particles. The selection of this two representative powder particle sizes is related to the experimentally obtained results. It was seen in Fig. 8 that there is a significant difference between the PSD of virgin powder and the one collected at the nozzle exit in the tube tests. The following analysis is aimed at studying the flow of the smallest and largest particles in order to explain this difference in PSD distribution. 1 µm and 130 µm particles were selected as representative of each group. As it is seen in the figure, nozzle exit and the tube employed in the actual experimental tests were also modelled and integrated in the simulation system. From the simulation results, it is concluded that small particles flow away from the tube while all big particles are predicted to be collected inside the tube. Simulations results shown in this section are focused on the performance of smallest and largest powder sizes only because it is in these ones where main changes were observed in the experimental tests.

Simulation results shown in Fig. 9 are in good agreement with powder size distribution of particles experimentally collected at the nozzle exit (Fig. 8).

In order to further analyse the trajectories of powder particles and explain the PSD obtained at the nozzle exi in the tube test, Fig. 10 shows the trajectories followed by 1 µm (Fig. 10 (a)) and 130 µm (Fig. 10 (b)) particles. As it is seen, smallest particles flow away from the deposition area (in this case the tube area), while most of the biggest particles are predicted to converge in the tube.

The particular characteristics of small particles (<10 µm) has been noted by previous authors in the literature [36]. This particles move with gas flows and are difficult or even impossible to collect at the nozzle exit. However, it was seen that the proposed model could predict well the trajectory of these particles.

As mentioned above, all the predictions are based on a first calculation to obtain the relative velocity of powder particles during the powder flow based on initial process parameter values. In order

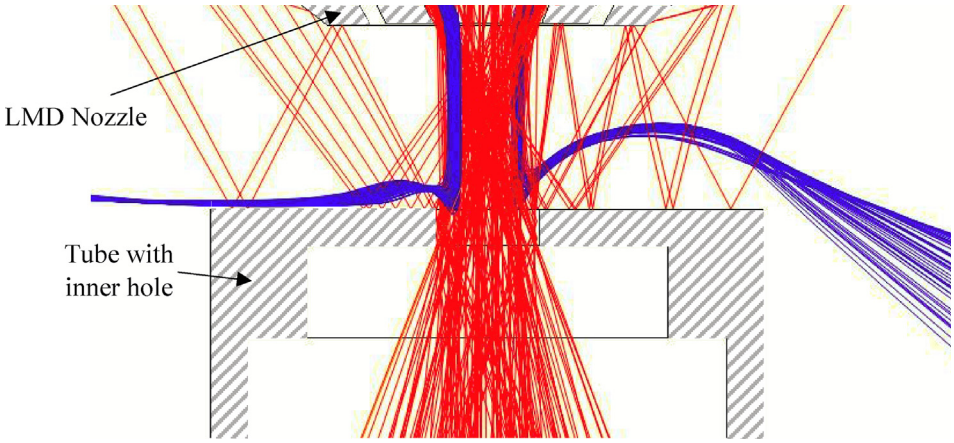

Fig. 9. 2D Trajectory of powder particles outside the nozzle. Blue and red lines correspond to 1 µm and 130 µm powder particles, respectively. (For interpretation of the references to color in this figure legend, the reader is referred to the web version of this article.)

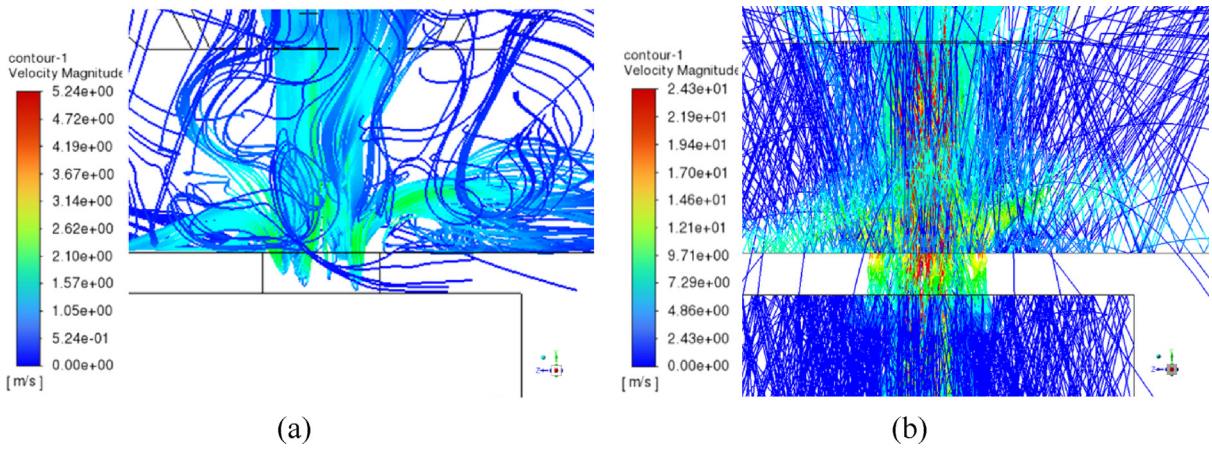

Fig. 10. 3D Powder particle's flow paths: (a) 1 μm and (b) 130 μm.

to analyze contact and collision between powders in the following steps, only relative velocity between powders is needed, therefore, in the following only relative velocity of particles will be considered. Fig. 11 shows the relative velocity of the powder obtained along its trajectory for 130 μm powder particles. Concretely, relative velocity of 20 randomly chosen particles is shown in the figure, each color representing the velocity achieved by a different particle. This calculation was conducted with ANSYS Fluent software.

Powder velocity on Z direction is considered as it is the direction in which the collision between powders is forced to occur. Nozzle exit is taken as the origin of this trajectory (0 value in X label). Values to the left of the origin (negative values) correspond to positions of the powder inside the nozzle, while positive values are positions once the powder is outside the nozzle. It is observed that a significant amount of powder achieves its maximum relative velocity near the nozzle exit.

3.2. STRESS DISTRIBUTION AND DENT FORMATION

Based on the velocity fields obtained in the previous step, collision between powder particles is analyzed through another simulation with ANSYS Explicit Dynamics. Particles are forced to collide in Z direction and the generated stress field as consequence of the collision is calculated through Johnson-Cook model for high-strain-rate simulation [37]. Concretely, one particle is considered fixed in x and y directions and free to move in z and the other one is moved for collision. The arising stresses are calculated considering the relative velocity between particles. As both particles are of the same material, both will deform, which will decrease the impact energy. A 10 μm meshing element size is applied to the spheres that represent the powder particles and an adaptive sizing is considered to smooth the mesh. The rest of meshing parameters were left as default. Fig. 12 shows an example of the stress field in a powder particle after collision. Concretely, the stress distribution after collision between two particles with a relative velocity of 18 m/s is shown. This relative velocity was selected for the following analysis because is the highest relative velocity value that was obtained as result of the particle flow analysis (see Fig. 11).

At this stage and considering the stress field presented above, plastic deformation of the particles as consequence of the collision can be calculated as well. As it is seen in Fig. 13 this plastic deformation is actually dent formation. The dent shown in the figure was predicted considering an 18 m/s relative velocity between colliding particles. Details about dent dimensions are also included in the figure.

In order to validate the prediction of dent formation, dent radius calculations conducted in this study were compared to those published in the literature by Alexander et al. [38] under

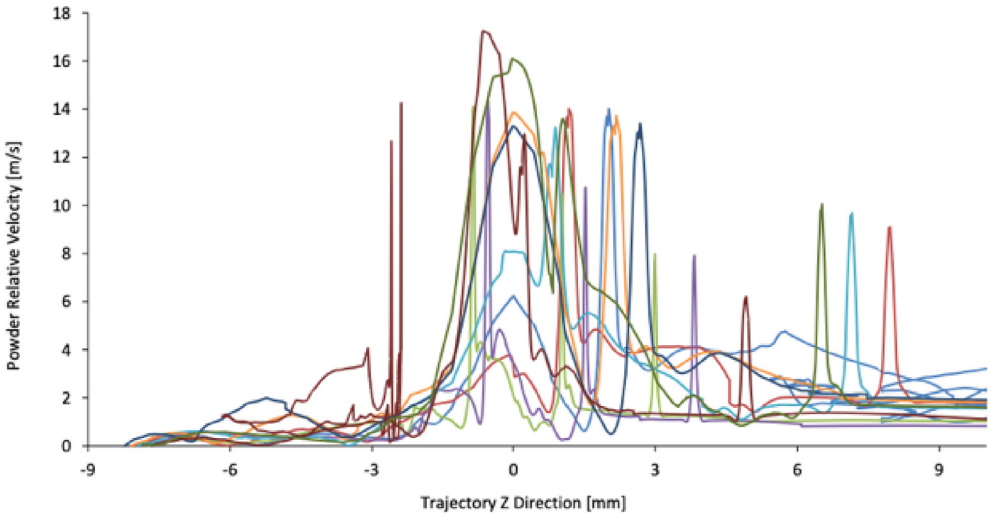

Fig. 11. Relative velocity of twenty 130 μm powder particles simulated in ANSYS Fluent. Each color represents a different particle.

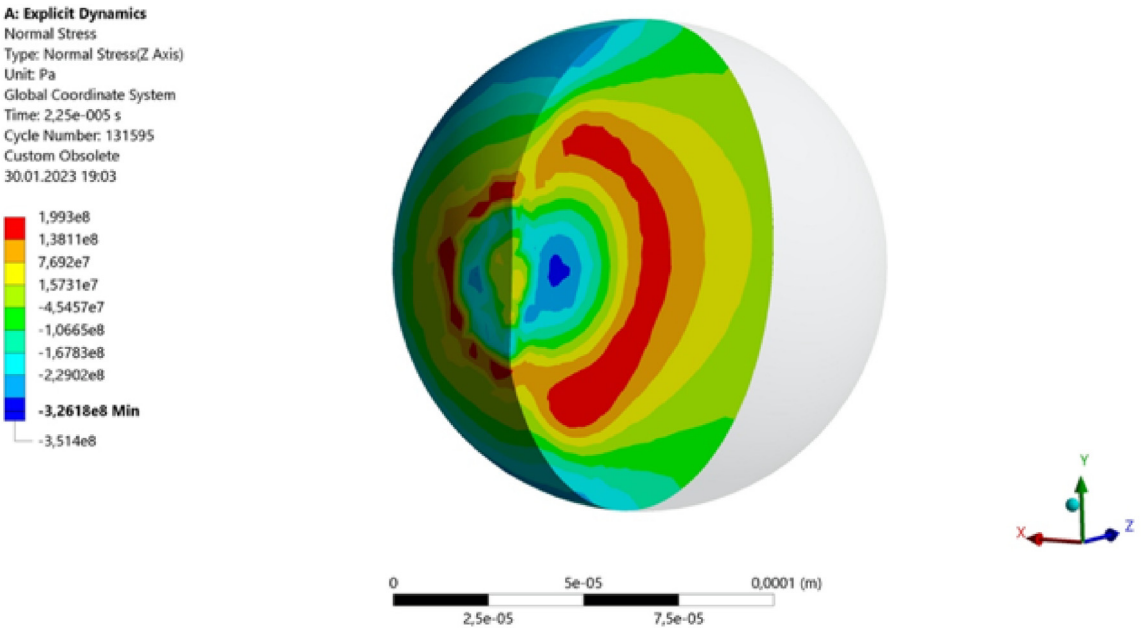

Fig. 12. Stress values obtained after simulation of 130 μm particle collision in ANSYS Explicit considering an 18 m/s relative velocity.

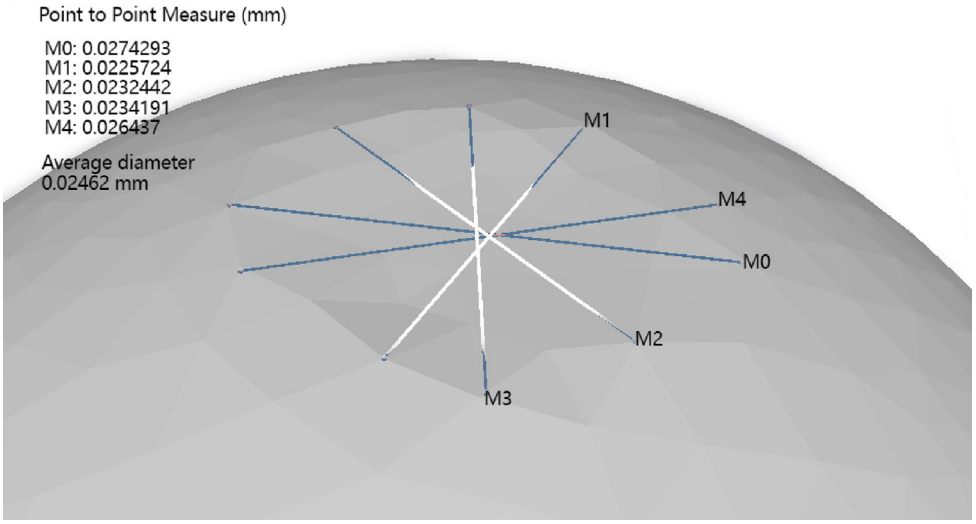

Fig. 13. Simulated dent formation and its dimensions (mm) for the 130 μm particle with 18 m/s relative velocity.

the same process conditions. Fig. 14 shows the contact radius a calculated through this model as $a^* = \frac{a_{dent}}{R_1}$, where a_{dent} is the dent size and R_1 is the particle diameter and the ones published by the authors mentioned above. As it is seen, the model employed in the present study is able to predict well the dent size.

Additionally, the prediction of dent formation provided by the model was compared with the characteristics of the experimentally collected powder particles. Fig. 15 shows SEM images of powder collected in the tubes at the exit of the nozzle.

It is clearly seen in Fig. 15 (a) that the morphology of powder particles changed after they exit the nozzle. The particles are no longer spherical after the interaction with the nozzle and between each other. Fig. 15 (b) shows dents formed in a particular powder particle collected at the nozzle exit. Diameter of the dents were measured and values of the marked dents are (1) 12.68 μm, (2) 12.34 μm and (3)13.58 μm. Comparing both the experimental results shown in Fig. 15 (b) and the model prediction (Fig. 13), it can be stated that the model predicts well the dent formation for a given relative velocity of powders although dent dimensions are slightly overestimated.

3.3. PARTICLE AGGLOMERATION

In an effort to explain the high amount of big particles collected at the nozzle exit, the analysis of particle agglomeration phenomena was integrated in the numerical model.

Firstly, in order to add the powder bouncing phenomena to the simulation, the model proposed by Collin and Zemin [33] is integrated. The critical plastic adhesive sticking velocity (V_{Crit}^{CZ}) is much larger than the adhesive sticking without considering plastic deformation predicted by JKR theory, and the difference increases with

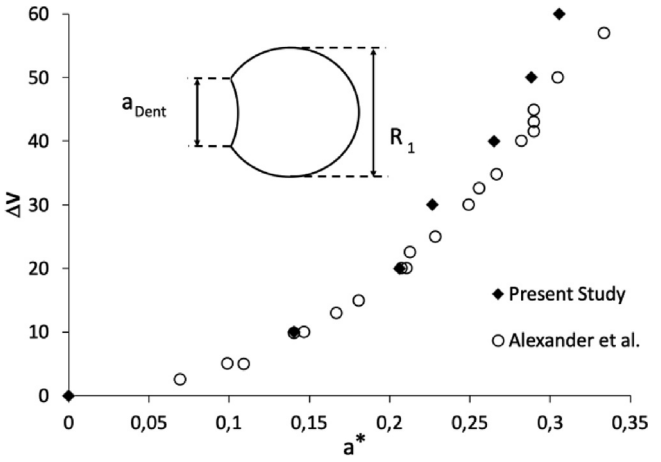

Fig. 14. Validation of dent radius depending on the relative velocity of particles [38].

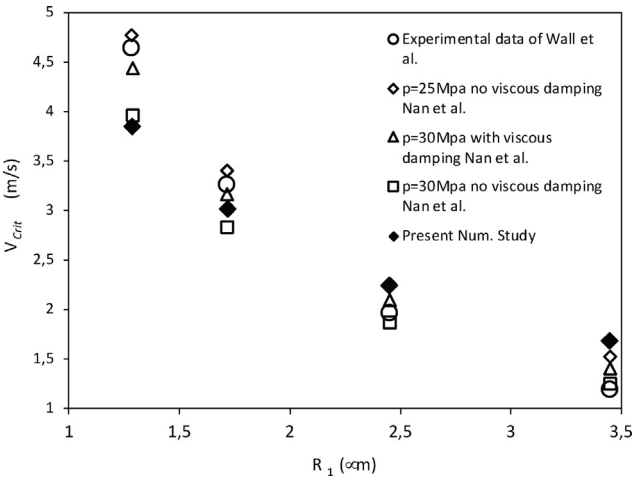

Fig. 16. Evaluation of contact between powders.

the decrease in particle size [39]. The critical sticking velocity V_{Crit}^{CZ} without bouncing is given by the following expressions:

$$\frac{1}{m^*} = \frac{1}{m_1} + \frac{1}{m_2} \tag{3}$$

$$V^{CZ}{}_{Crit} = \left(\frac{14.18}{m^*}\right)^{\frac{1}{2}} \left(\frac{\Gamma^5 R^{*4}}{E^{*2}}\right)^{\frac{1}{6}} \tag{4}$$

where m^* is normalized powder mass (Eq. (2)) and E^* and Γ are the normalized Young modulus and surface energy, respectively (Eq. (3)). As for the surface energy, Ning used 0.2 for surface energy (Γ) and Du et al. chose 1.0 in his calculations [39]. Abhirup et al. measured different material surface energies and the range of the surface energy in his study is 1.08 – 3.19 J/m^2 [39,40]. In this model, a surface energy of 1 J/m^2 was considered as the minimum value for metals.

Taking all those expressions into account, particle collision and bouncing was further analyzed. Fig. 16 shows a comparison of critical velocity (V_{crit}) values above which particles are assumed to bounce back after collision. R_1 values on the X axis refer to powder sizes. Only small size powders are analyzed because it is known that small particles are the ones that adhere to the big ones. This will be shown later in the simulation results as well. Values predicted in the present work (represented as diamonds) are compared to other simulated and experimental values extracted from the literature. It can be seen that values predicted are in good agreement with those find in other studies. It is worth noting that critical velocities for stable adhesion decrease with increasing powder size.

Once powder agglomeration was studied, it was also simulated through Rocky DEM application. Fig. 17 shows the powder stream simulated from the inside to the outside of the nozzle and a detailed image of the powder particles in that stream showing the agglomeration of particles.

Additionally, the size of agglomerated particles is also calculated and shown in Fig. 18. As seen in the figure, small particles (around 12 μm) are gathered together and adhere to the bigger ones (from 60 to 130 μm). This trend is due to the higher adhesion forces of the biggest particles (see Fig. 19). It is worth noting here that no adhesion between large particles and small particles was observed, the agglomeration was only between different particle sizes.

This simulation results were also compared to the experimental findings. Fig. 20 shows a detail of particle agglomeration observed at the nozzle exit.

Agglomeration type predicted by the model and shown in Fig. 18 and Fig. 19 is similar to the one experimentally observed

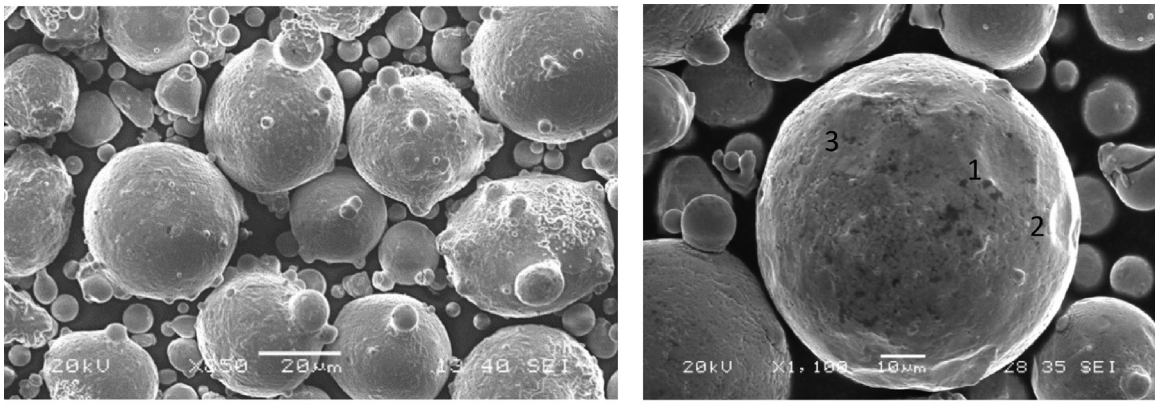

Fig. 15. SEM images of powder particles collected after the experimental tests, showing two different phenomenon: (a) particle agglomeration and (b) dent formation.

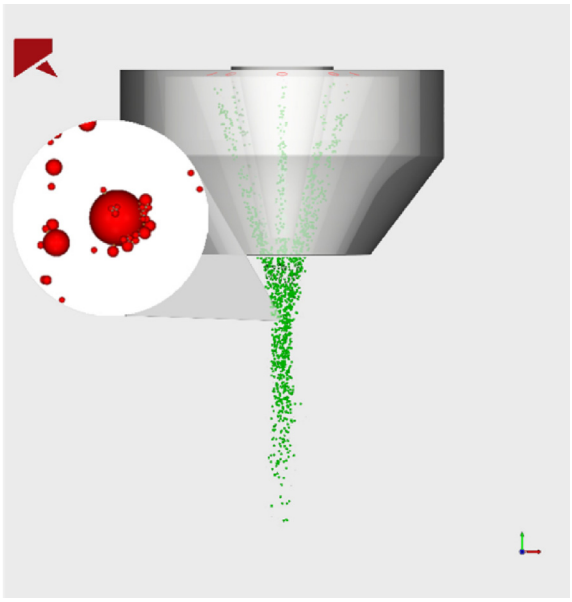

Fig. 17. Powder agglomeration simulation using Rocky DEM.

and highlighted in red in Fig. 20, which again validates the predictions obtained by the model proposed in this paper.

4. Conclusions

In this work, powder particle flow dynamics in LMD is studied to predict PSD distribution, dent formation and powder particle agglomeration at the exit of the nozzle. With this aim, simulations have been conducted using Ansys Fluent and Explicit software. Particle trajectory and relative velocities are first calculated taking into account the process parameter values (powder material, powder properties, powder flow rate, carrier gas flow rate, etc.). Powder particles are forced to collide and considering their relative velocities, stress fields and powder deformations (dent) are calculated based on the Johnson-Cook high-strain-rate model. Finally, particle agglomeration is analyzed integrating the adhesion phenomena through Johnson-Kendall-Roberts model. Results obtained in the simulations have been validated through experimental tests in which powder morphology at the LMD nozzle exit was analyzed through SEM images. From the results obtained in the simulations and the experimental tests, the following conclusions can be drawn:

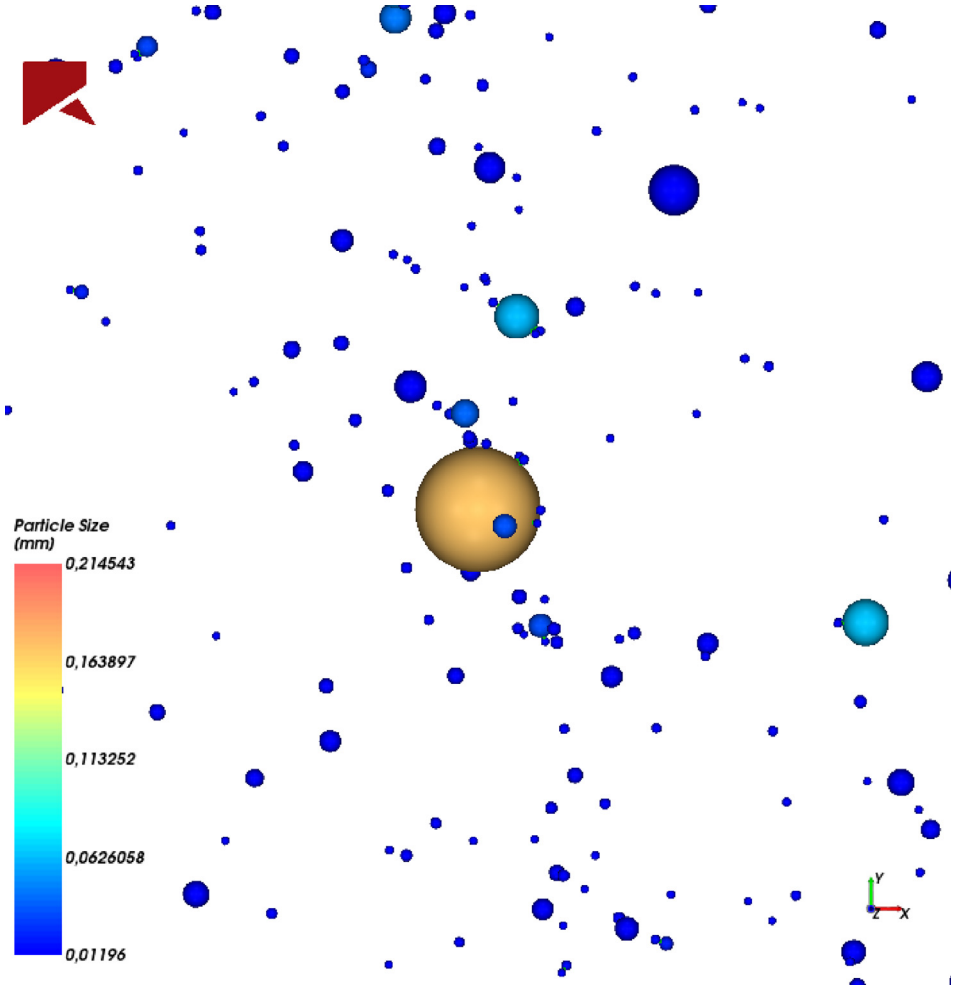

Fig. 18. Prediction of the agglomerated particle sizes.

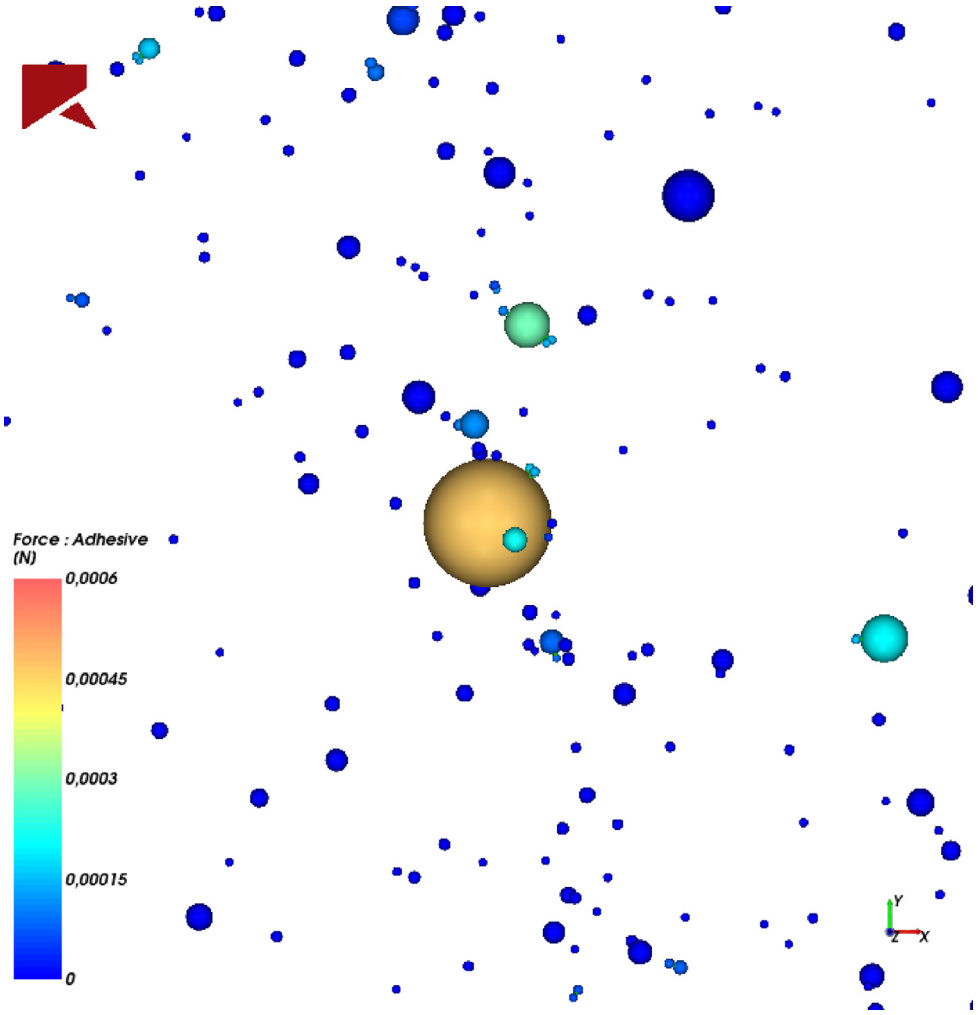

Fig. 19. Analysis of the adhesion forces obtained through the JKR model.

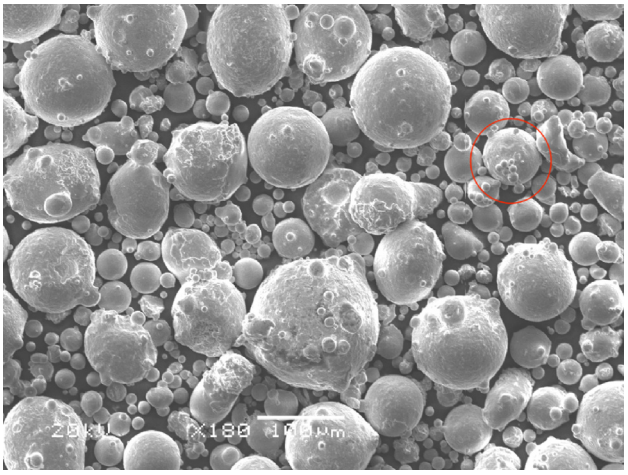

Fig. 20. Agglomeration between particles at nozzle exit.

- Only the large particles (>100 μm) are collected at the outside of the nozzle. Small particles (<10 μm) flow away from the deposition area.
- The dent formation is predicted using a numerical simulation model based on the relative velocity of the colliding particles with values close to what measured experimentally.
- It has been shown that small particles (around 12 μm) tend to agglomerate around the bigger ones (60–130 μm). This is due to the higher adhesion forces of the latest.
- In general, it has been shown that predictions made by the approach proposed fit well with the experimental results.

CRediT authorship contribution statement

Ahmet Guner: Conceptualization, Data curation, Formal analysis, Writing – original draft, Writing – review & editing. **Prveen Bidare:** Conceptualization, Data curation, Writing – review & editing. **Amaia Jiménez:** Data curation, Formal analysis, Writing – original draft, Writing – review & editing. **Chang Shu:** Data curation, Investigation. **Nikolina Kovacev:** Data curation, Investigation. **Khamis Essa:** Conceptualization, Writing – review & editing.

Declaration of competing interest

The authors declare that they have no known competing financial interests or personal relationships that could have appeared to influence the work reported in this paper.

References

[1] A. Azarniya et al., Additive manufacturing of Ti–6Al–4V parts through laser metal deposition (LMD): process, microstructure, and mechanical properties, J.

Alloys Compd. 804 (2019) 163–191, https://doi.org/10.1016/j.jallcom.2019.04.255.
[2] N. Shamsaei, A. Yadollahi, L. Bian, S.M. Thompson, An overview of direct laser deposition for additive manufacturing; Part II: mechanical behavior, process parameter optimization and control, Addit. Manuf. 8 (2015) 12–35, https://doi.org/10.1016/j.addma.2015.07.002.
[3] X. Zhang F. Liou, *Introduction to additive manufacturing*. Elsevier Inc., 2021.
[4] A. Guner, P. Bidare, A. Jiménez, S. Dimov, K. Essa, Nozzle designs in powder-based direct laser deposition: a review, Int. J. Precis. Eng. Manuf. 23 (9) (2022) 1077–1094, https://doi.org/10.1007/s12541-022-00688-1.
[5] Z. Jardon, P. Guillaume, J. Ertveldt, M. Hinderdael, G. Arroud, Offline powder-gas nozzle jet characterization for coaxial laser-based directed energy deposition, Procedia CIRP 94 (2020) 281–287, https://doi.org/10.1016/j.procir.2020.09.053.
[6] J. Lin, Concentration mode of the powder stream in coaxial laser cladding, Opt. Laser Technol. 31 (3) (1999) 251–257, https://doi.org/10.1016/S0030-3992(99)00049-3.
[7] J. Lin, Laser attenuation of the focused powder streams in coaxial laser cladding, J. Laser Appl. 12 (1) (2000) 28–33, https://doi.org/10.2351/1.521910.
[8] X. Gao, X.X. Yao, F.Y. Niu, Z. Zhang, The influence of nozzle geometry on powder flow behaviors in directed energy deposition additive manufacturing, Adv. Powder Technol. 33 (3) (2022), https://doi.org/10.1016/j.apt.2022.103487 103487.
[9] J. Lin, Numerical simulation of the focused powder streams in coaxial laser cladding, J. Mater. Process. Technol. 105 (1) (2000) 17–23, https://doi.org/10.1016/S0924-0136(00)00584-7.
[10] H. Pan, F. Liou, Numerical simulation of metallic powder flow in a coaxial nozzle for the laser aided deposition process, J. Mater. Process. Technol. 168 (2) (2005) 230–244, https://doi.org/10.1016/j.jmatprotec.2004.11.017.
[11] H. Pan, T. Sparks, Y.D. Thakar, F. Liou, The investigation of gravity-driven metal powder flow in coaxial nozzle for laser-aided direct metal deposition process, J. Manuf. Sci. Eng. Trans. ASME 128 (2) (2006) 541–553, https://doi.org/10.1115/1.2162588.
[12] L. Li, Y. Huang, and C. Paper, "Numerical and Experimental Study on Powder Stream Characteristics in CoaxialLaser Cladding Process," *6th Int. Conf. Weld. Sci. Eng. Biejing, China*, no. October, pp. 2–6, 2015, [Online]. Available: https://www.researchgate.net/profile/Li_qun_Li/publication/282301105_Numerical_and_Experimental_Study_on_Powder_Stream_Characteristics_in_ CoaxialLaser_Cladding_Process/links/560b475b08ae576ce6411017.pdf.
[13] Y. Xia, Z. Huang, H. Chen, X. Liang, J. Lei, Numerical simulation and experimental investigation on powder transport of a new-type annular coaxial nozzle, Int. J. Adv. Manuf. Technol. 115 (7–8) (2021) 2353–2364, https://doi.org/10.1007/s00170-021-07294-x.
[14] S. Zekovic, R. Dwivedi, R. Kovacevic, Numerical simulation and experimental investigation of gas-powder flow from radially symmetrical nozzles in laser-based direct metal deposition, Int. J. Mach. Tools Manuf. 47 (1) (2007) 112–123, https://doi.org/10.1016/j.ijmachtools.2006.02.004.
[15] S.Y. Wen, Y.C. Shin, J.Y. Murthy, P.E. Sojka, Modeling of coaxial powder flow for the laser direct deposition process, Int. J. Heat Mass Transf. 52 (25–26) (2009) 5867–5877, https://doi.org/10.1016/j.ijheatmasstransfer.2009.07.018.
[16] A. Zhang, D. Li, Z. Zhou, G. Zhu, B. Lu, Numerical simulation of powder flow field on coaxial powder nozzle in laser metal direct manufacturing, Int. J. Adv. Manuf. Technol. 49 (9–12) (2010) 853–859, https://doi.org/10.1007/s00170-010-2657-8.
[17] S. Morville *et al.*, "Numerical Modeling of Powder Flow during Coaxial Laser Direct Metal Deposition – Comparison between Ti-6Al-4V Alloy and Stainless Steel," *2012 COMSOL Conf. Milan*, 2012, [Online]. Available: http://www.comsol.com/paper/numerical-modeling-of-powder-flow-during-coaxial-laser-direct-metal-deposition-c-13191.
[18] S. Takemura, R. Koike, Y. Kakinuma, Y. Sato, Y. Oda, Design of powder nozzle for high resource efficiency in directed energy deposition based on computational fluid dynamics simulation, Int. J. Adv. Manuf. Technol. 105 (10) (2019) 4107–4121, https://doi.org/10.1007/s00170-019-03552-1.
[19] P. Nie, O.A. Ojo, Z. Li, Modeling analysis of laser cladding of a nickel-based superalloy, Surf. Coatings Technol. 258 (2014) 1048–1059, https://doi.org/10.1016/j.surfcoat.2014.07.030.
[20] B.A. Khamidullin, I.V. Tsivilskiy, A.I. Gorunov, A.K. Gilmutdinov, Modeling of the effect of powder parameters on laser cladding using coaxial nozzle, Surf. Coatings Technol. 364 (May 2019) (2018) 430–443, https://doi.org/10.1016/j.surfcoat.2018.12.002.
[21] L.-C. Zhang, W.-Y. Xu, Z. Li, L. Zheng, Y.-F. Liu, G.-Q. Zhang, Mechanism of rapidly solidified satellites formation in gas atomized powders: simulation and characterization, Powder Technol. 418 (December 2022) (2022) 118162, https://doi.org/10.1016/j.powtec.2022.118162.
[22] J.L. Sinclair, R. Jackson, Gas-particle flow in a vertical pipe with particle-particle interactions, AIChE J. 35 (9) (1989) 1473–1486, https://doi.org/10.1002/aic.690350908.
[23] X.Y. Sun, X.W. Cao, Impact of inter-particle collision on elbow erosion based on DSMC-CFD method, Pet. Sci. 18 (3) (2021) 909–922, https://doi.org/10.1007/s12182-021-00550-5.
[24] A.D. Salman, C.A. Biggs, J. Fu, I. Angyal, M. Szabó, M.J. Hounslow, An experimental investigation of particle fragmentation using single particle impact studies, Powder Technol. 128 (1) (2002) 36–46, https://doi.org/10.1016/S0032-5910(02)00151-1.
[25] Y. Rozenblat, E. Grant, A. Levy, H. Kalman, J. Tomas, Selection and breakage functions of particles under impact loads, Chem. Eng. Sci. 71 (2012) 56–66, https://doi.org/10.1016/j.ces.2011.12.012.
[26] X. Wang, J. Shi, Validation of Johnson-Cook plasticity and damage model using impact experiment, Int. J. Impact Eng. 60 (2013) 67–75, https://doi.org/10.1016/j.ijimpeng.2013.04.010.
[27] O.B. Kovalev, I.O. Kovaleva, I.Y. Smurov, Numerical investigation of gas-disperse jet flows created by coaxial nozzles during the laser direct material deposition, J. Mater. Process. Technol. 249 (May) (2017) 118–127, https://doi.org/10.1016/j.jmatprotec.2017.05.041.
[28] H. Liu et al., "Numerical simulation of powder transport behavior in laser cladding with coaxial powder feeding,", Sci. China Physics, Mech. Astron. 58 (10) (2015), https://doi.org/10.1007/s11433-015-5705-4.
[29] H.K. Farahani, M. Ketabchi, S. Zangeneh, Determination of johnson-cook plasticity model parameters for inconel718, J. Mater. Eng. Perform. 26 (11) (2017) 5284–5293, https://doi.org/10.1007/s11665-017-2990-2.
[30] D. Maugis, H.M. Pollock, Surface forces, deformation and adherence at metal microcontacts, Acta Metall. 32 (9) (1984) 1323–1334, https://doi.org/10.1016/0001-6160(84)90078-6.
[31] A.P. Alkhimov, S.V. Klinkov, V.F. Kosarev, Experimental study of deformation and attachment of microparticles to an obstacle upon high-rate impact, J. Appl. Mech. Tech. Phys. 41 (2) (2000) 245–250.
[32] W. Nan, W.P. Goh, M.T. Rahman, Elasto-plastic and adhesive contact: an improved linear model and its application, Powder Technol. 407 (2022), https://doi.org/10.1016/j.powtec.2022.117634.
[33] C. Thornton, Z. Ning, A theoretical model for the stick/bounce behaviour of adhesive, elastic- plastic spheres, Powder Technol. 99 (2) (1998) 154–162, https://doi.org/10.1016/S0032-5910(98)00099-0.
[34] K.L. Johnson, K. Kendall, A.D. Roberts, Surface energy and the contact of elastic solids, Proc. R. Soc. London. A. Math. Phys. Sci. 324 (1558) (1971) 301–313, https://doi.org/10.1098/rspa.1971.0141.
[35] S. Kook, M.K. Le, S. Padala, E.R. Hawkes, "Z-type schlieren setup and its application to high-speed imaging of gasoline sprays,", SAE Tech. Pap. (August) (2011), https://doi.org/10.4271/2011-01-1981.
[36] P. Lösch, K. Nikolaus, S. Antonyuk, Fractionating of finest particles using cross-flow separation with superimposed electric field, Sep. Purif. Technol. 257 (October) (2020) 2021, https://doi.org/10.1016/j.seppur.2020.117820.
[37] G.R. Johnson, W.H. Cook, Fracture characteristics of three metals subjected to various strains, strain rates, temperatures and pressures, Eng. Fract. Mech. 21 (1) (1985) 31–48, https://doi.org/10.1016/0013-7944(85)90052-9.
[38] A. Strobel, B. Köninger, S. Romeis, F. Schott, K.E. Wirth, W. Peukert, Assessing stress conditions and impact velocities in fluidized bed opposed jet mills, Particuology 53 (2020) 12–22, https://doi.org/10.1016/j.partic.2020.02.006.
[39] W. Nan, W.P. Goh, M.T. Rahman, Elasto-plastic and adhesive contact: an improved linear model and its application, Powder Technol. 407 (June) (2022), https://doi.org/10.1016/j.powtec.2022.117634 117634.
[40] A. Patra, J.E. Bates, J. Sun, J.P. Perdew, Properties of real metallic surfaces: effects of density functional semilocality and van der Waals nonlocality, Proc. Natl. Acad. Sci. U. S. A. 114 (44) (2017) E9188–E9196, https://doi.org/10.1073/pnas.1713320114.